This article has been accepted for publication in IEEE Journal of Emerging and Selected Topics in Industrial Electronics. This is the author's version which has not been fully edited and content may change prior to final publication. Citation information: DOI 10.1109/JESTIE.2024.3425518



# Voltage control of the Ćuk converter for grid-forming in DC grids: An energy-based approach

Marco Guerreiro, Pedro dos Santos, and Steven Liu, *Member, IEEE*

***Abstract*—Grid-forming converters in DC microgrids will have a key role in the next generation power system. These converters are responsible for stabilizing the bus voltage in a grid dominated by constant power loads, a task that requires highly dynamic voltage control loops. This paper presents an energy-based method to control the output voltage of an isolated Ćuk converter, a high-order nonlinear system. The main motivation behind the energy-based method is to control the total energy of the converter. In many cases, most of the energy is stored in the output capacitor of the converter, and controlling total energy allows shaping the output voltage directly. By using feedback linearization, we show that it is possible to use a linear controller to control energy, and that the internal dynamics resulting from feedback linearization is stable. The energy-based method results in a single-loop controller capable of naturally handling constant power loads, characteristics that make it well suited for voltage control of grid-forming converters. The proposed controller is verified by experimental results, using an isolated Ćuk converter to supply a constant power load.**

***Index Terms*—DC microgrids, grid-forming control, grid-forming converters, energy control, feedback linearization.**

## I. Introduction

To improve efficiency, resilience and sustainability, the current power system is shifting from today's centralized generation paradigm to a renewable-based distributed one [1], [2]. One way to handle this new paradigm is with microgrids, small power systems consisting of local generation and loads [3], [4]. Microgrids have key characteristics that are well aligned with the the next generation power system: a microgrid achieves better efficiency by supplying local loads with local generation, improved resilience since it can operate isolated from the main grid during faults, and sustainability by integrating renewable-based generation.

While AC microgrids are more common due to compatibility with existing infrastructure, DC microgrids have gained increasing attention as a more efficient alternative, due to the DC nature of many renewable sources, energy storage systems and loads [5], [6]. DC grids also avoid some of the control challenges of AC systems, such as frequency and reactive power control. Currently, the main challenges faced by implementation of DC microgrids are lack of standards and lack of protection equipment, active topics in both industry [7] and academia [8].

Forming a DC microgrid requires setting and stabilizing the main DC bus voltage, a process called grid forming [9]. Units responsible for grid forming work in voltage control mode and stabilize the bus voltage by balancing generation and demand, and additional controllers are used to provide the voltage reference in order to regulate voltage and power flow in the microgrid [10], [11]. For this reason, the voltage controller must be able to handle power steps at the output of the converter, as well as steps in its reference voltage.

The Ćuk converter is an interesting topology for grid forming applications. The possibility to achieve zero current ripple on the inductors reduces electromagnetic interference emissions and reduces the output voltage ripple [12], [13], which is especially important for grid applications. This converter has been studied for interfacing renewables with the grid [14]–[16], and, with increasing interest in using renewables for grid forming [17], [18], it is essential to develop voltage control methods for the Ćuk converter that are able to handle the grid-forming task.

Using Ćuk converter as a grid-forming unit is challenging because the converter is a high-order nonlinear system presenting nonminimum phase behavior between control input and output voltage. This behavior complicates or even prevents the use of classical nonlinear control techniques to control output voltage directly, such as sliding mode control and feedback linearization [19]. Feedback linearization is an especially interesting nonlinear technique, because it transforms a nonlinear system into a linear one [20], [21]. However, feedback linearization is mostly used to control the input current of the Ćuk converter (the only state showing minimum phase behavior), which affects the output voltage only indirectly. Thus, an additional loop is required to control the output voltage, resulting in a inherently slower controller.

To leverage feedback linearization for the Ćuk converter for output voltage control, it is necessary to find a system output that directly affects the output voltage. One such output is the total energy of the converter, which, in many practical cases, is mostly stored in the output capacitor. Controlling total energy is then approximately the same as controlling the energy of the output capacitor and, hence, the output voltage.

Energy shaping of the Ćuk converter has been investigated before in the context of passivity-based control (PBC), and in-

Manuscript received xxx. This research was made possible by funding from the Carl-Zeiss-Stiftung

The authors are with the Chair of Control Systems, University of Kaiserslautern-Landau, Kaiserslautern, Germany (e-mails: marco.guerreiro@rptu.de, pdsantos@rptu.de, steven.liu@rptu.de)

This article has been accepted for publication in IEEE Journal of Emerging and Selected Topics in Industrial Electronics. This is the author's version which has not been fully edited and content may change prior to final publication. Citation information: DOI 10.1109/JESTIE.2024.3425518



terconnection and damping assignment PBC (IDA-PBC) [22]–[24]. In PBC, the main goal is to shape the energy stored in the converter by changing how the system dissipates energy. The main limitation of PBC is that the passive output must be minimum phase [25]. IDA-PBC is an extension of PBC and overcomes the minimum phase requirement [26], [27]. However, the main challenge of using IDA-PBC is synthesizing the controller, which often requires solving nonlinear partial differential equations.

In this paper, we explore the idea of using energy to control the output voltage of the Ćuk converter. We show that it is possible to use feedback linearization to control energy with a linear controller, which can be designed based on control requirements such as settling time and overshoot. Because feedback linearization partially transforms the Ćuk converter in a linear system, operation and design of the linear controller is not restricted to an operating point, leading to a more dynamic voltage control and, thus, a more dynamic grid-forming control. We show that the energy-based approach naturally handles constant power loads (CPLs), a very common type of load in microgrids. Moreover, a stability analysis is provided, where it is shown that the closed-loop system is stable for arbitrary positive output power. The main advantages of the proposed method are the possibility to control voltage with a single control loop, ability to handle CPLs, simpler design based on linear control theory, and fully digital implementation. This is in contrast with previous voltage controllers reported in the literature that either consist of cascaded loops [19], [23], [26], have complex hardware implementation [28], or have complex design procedures [29].

This paper is organized as follows. Section II discusses energy control of the Ćuk converter using feedback linearization, and shows a stability analysis. Section III shows the validation of the energy controller with experimental results. The controller is verified with focus on typical scenarios faced by grid-forming units: power steps from a CPL, and steps in the reference voltage. Section IV concludes the paper.

## II. Energy Control of the Ćuk Converter

This section discusses using energy to control the output voltage of the Ćuk converter, and is divided into three parts. The first part shows the model of the isolated Ćuk converter, the second part discusses energy control and its usage for voltage control, and the third part provides a stability analysis.

### A. Isolated Ćuk converter model

The isolated Ćuk converter is shown in Fig. 1. The converter is supplied by a constant voltage source with voltage $V_\mathrm{i}$. $L_1$ and $L_2$ are the input and output inductors, with currents $i_1$ and $i_2$; $C_1$ and $C_2$ are the coupling capacitors, with voltages $v_1$ and $v_2$; $C_\mathrm{o}$ is the output capacitor, with voltage $v_\mathrm{o}$; and the load is a CPL represented by a current source with current $i_\mathrm{o} = P_\mathrm{o}/v_\mathrm{o}$, where $P_\mathrm{o}$ is the power of the load. The primary and secondary sides of the converter are coupled by an ideal transformer with a turn ratio between primary and secondary of 1 : N. Switches $S_1$ and $S_2$ operate in a complementary fashion and are used to control the converter.

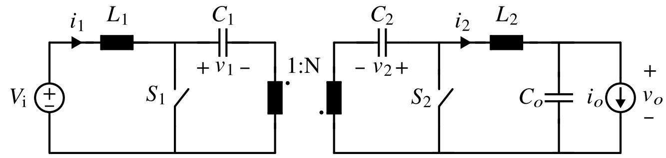


Fig. 1: Isolated Ćuk converter.

For analysis and control purposes, we assume an average model of the converter. The control input for the average model is the duty-cycle $u$ of switch $S_1$. Furthermore, it is assumed that $C_1 = C_2 = C_\mathrm{c}$. Defining $v_\mathrm{c} = v_1 + (1/N)v_2$, the average model of the converter is represented by:

$$L_1\dot{i}_1 = -v_\mathrm{c}(1-u) + V_\mathrm{i}, \tag{1a}$$
$$L_2\dot{i}_2 = Nv_\mathrm{c}u - v_\mathrm{o}, \tag{1b}$$
$$\left(\frac{N^2}{N^2+1}\right) C_\mathrm{c}\dot{v}_\mathrm{c} = i_1(1-u) - Ni_2u, \tag{1c}$$
$$C_\mathrm{o}\dot{v}_\mathrm{o} = i_2 - i_\mathrm{o}. \tag{1d}$$

### B. Control design

Designing the energy control system for the Ćuk converter consists of two steps. In the first step, feedback linearization is used to control the converter's total energy. By using feedback linearization, the Ćuk converter is partially transformed to a double-integrator system, where the states are the converter's total energy and power. In the second step, a linear state-feedback controller is designed to control this double integrator system, and pole placement is used to design the controller according to settling time and overshoot specifications.

In cases where the total energy of the converter is mostly stored in the output capacitor, controlling energy allows controlling the output voltage directly. Thus, the dynamics of the output voltage is approximately described by the energy dynamics. Because of the nonlinear transformation introduced by feedback linearization, energy can in principle be controlled to meet arbitrary settling time and overshoot specifications. However, in practice, this will be limited by physical constraints of the converter. A very dynamic energy control would require large input currents and may saturate the duty-cycle.

This section gives a brief introduction to input-output feedback linearization, discusses its use to control energy, and discusses practical limitations of the method.

*1) Input-output feedback linearization:* We restrict our attention to single-input single-output (SISO) systems. Furthermore, we focus on the case where the relative degree is less than the order of the system. For a more complete discussion on feedback linearization, the reader is referred to [21].

The problem is finding a control law that linearizes a chosen system output with respect to an auxiliary (virtual) input. Consider the nonlinear, $n$-th order input-affine SISO system

$$\dot{x} = f(x) + g(x)u, \tag{2a}$$
$$y = h(x), \tag{2b}$$

where $x \in \mathbb{R}^n$ is the state vector, $u \in \mathbb{R}$ is the control signal, $y \in \mathbb{R}$ is the output, and $f : D \to \mathbb{R}^n$, $g : D \to \mathbb{R}^n$, and

$h : D \to \mathbb{R}$ are smooth functions in some domain $D \in \mathbb{R}^n$. If there exists in $D$ a transform $T(x)$, with a respective change of variable $z = T(x)$, $z \in \mathbb{R}^n$, of the form

$$z = T(x) = \begin{bmatrix} \eta \\ \cdots \\ \xi \end{bmatrix} = \begin{bmatrix} \phi_1(x) \\ \vdots \\ \phi_{n-r}(x) \\ \cdots\cdots\cdots \\ h(x) \\ L_f h(x) \\ \vdots \\ L_f^{r-1} h(x) \end{bmatrix}, \tag{3}$$

that is bijective, continuously differentiable, has a continuously differentiable inverse, and such that $(\partial\phi_i(x)/\partial x)g(x) = 0$ $(1 \le i \le n - r)$, where $r$ is the relative degree, $L_f^k h(\mathbf{x})$ is the $k$-th Lie derivative of $h$ with respect to $f$, the system is input-output linearizable. The input transformation

$$u = \frac{-L_f^{\rho} h(x) + v}{L_g L_f^{\rho-1} h(x)}, \tag{4}$$

where $v \in \mathbb{R}$ is an auxiliary signal, leads to a chain of $\rho$ integrators given by

$$y^{(\rho)} = v, \tag{5}$$

where $y^{(\rho)}$ is the $\rho$-th derivative of $y$. The change of variables (3) along with input transformation (4) transform system (2) into the system:

$$\dot{\eta} = \frac{\partial \phi}{\partial x} f(x)\Big|_{x=T^{-1}(z)}, \tag{6a}$$
$$\dot{\xi} = A\xi + Bv, \tag{6b}$$
$$y = C\xi, \tag{6c}$$

where $A$, $B$, and $C$ represent the canonical form of a chain of $\rho$ integrators, and $\phi(x) = \begin{bmatrix}\phi_1(x) & \cdots & \phi_{n-r}(x)\end{bmatrix}^T$. Subsystem (6b)-(6c) is the chain of integrators resulting from using input-output feedback linearization, and can be controlled using a linear controller. Subsystem (6a) consists of $n - r$ states that are unobservable from the output, and is denoted as internal dynamics. If the internal dynamics is asymptotically stable around the equilibrium point of interest, system (6) is said to be minimum phase.

In practice, applying feedback linearization to a system consists of defining the system output, and taking its time derivative until the control signal appears in the resulting equation. Then, it is possible to find a linearizing feedback law that creates a linear relationship between the $\rho$-th time derivative of the output, and some virtual input $v$. This creates a chain of $\rho$ integrators between the output and $v$, and results in the linear system (6b)-(6c). The remaining part of the transform can be determined by using the condition that $(\partial\phi_i(x)/\partial x)g(x) = 0$. With the full transform, system (6a) (the internal dynamics) can be verified for stability. In practice, feedback linearization only makes sense if the internal dynamics is stable; otherwise, some states of the system would be unbounded.

*2) Energy control with input-output feedback linearization:* The goal is to define the system output as total energy, and find a linearizing feedback law $u$ that creates a linear relationship between a virtual signal $v$ and total energy. For a more concise notation, we rewrite the states of the Ćuk converter as defined in (1) in terms of the state vector $x = \begin{bmatrix}x_1 & x_2 & x_3 & x_4\end{bmatrix}^T$, where $x_1 = i_1$, $x_2 = i_2$, $x_3 = v_c$, and $x_4 = v_o$. The system output $y$ is defined as the total energy of the converter:

$$y = \frac{L_1}{2}x_1^2 + \frac{L_2}{2}x_2^2 + \frac{C_c}{2}\left(\frac{N^2}{N^2+1}\right)x_3^2 + \frac{C_o}{2}x_4^2. \tag{7}$$

The first time derivative of (7) is obtained as follows. Physically, if $y$ is the converter's energy, its time derivative $\dot{y}$ is the converter's power. This can be written as the difference between input and output power:

$$\dot{y} = V_i x_1 - P_o, \tag{8}$$

where the product $V_i x_1$ is the input power of the converter, and $P_o$ is the power of the load. Since the control signal $u$ does not appear in (8), the time derivative of $\dot{y}$ is taken. If $V_i$ is constant and the converter supplies a constant power load, then $\dot{P}_o = 0$ and $\ddot{y}$ is

$$\ddot{y} = \frac{V_i}{L_1}\big(-x_3(1-u) + V_i\big). \tag{9}$$

Based on (9), the following feedback law $u$ creates a linear relationship between a virtual signal $v$ and $\ddot{y}$:

$$u = 1 - \frac{L_1}{V_i x_3}\left(\frac{V_i^2}{L_1} - v\right). \tag{10}$$

Applying (10) in (9) yields

$$\ddot{y} = v, \tag{11}$$

which gives a linear relationship between virtual input $v$ and $\ddot{y}$ as a double integrator system. The linearized system can now be written as

$$\begin{bmatrix}\dot{y} \\ \ddot{y}\end{bmatrix} = \begin{bmatrix}0 & 1 \\ 0 & 0\end{bmatrix}\begin{bmatrix}y \\ \dot{y}\end{bmatrix} + \begin{bmatrix}0 \\ 1\end{bmatrix}v, \tag{12}$$

where the states of the linearized system are $y$ and $\dot{y}$, namely the converter's total energy and power. This system corresponds to subsystem (6b)-(6c).

The control problem now becomes that of controlling system (12). In this paper, a state feedback controller

$$v = -k_1 y - k_2 \dot{y} + k_1 y^* \tag{13}$$

is used, where $y^*$ is a setpoint for energy, and $k_1$ and $k_2$ are the controller gains. Via pole placement, gains $k_1$ and $k_2$ can be obtained to stabilize system (12) and to additionally meet control specifications for a second-order system, such as settling time and overshoot.

Controller (13) controls the converter's energy; in practice, we are interested in controlling the output voltage, and this can be achieved with a proper value for $y^*$. If $x_4^*$ is the setpoint for the output voltage, and the output power is known (measured), the energy setpoint can be defined as

$$y^* = \frac{L_1}{2}(x_1^*)^2 + \frac{L_2}{2}(x_2^*)^2 + \frac{C_c}{2}\left(\frac{N^2}{N^2+1}\right)(x_3^*)^2 + \frac{C_o}{2}(x_4^*)^2, \tag{14}$$

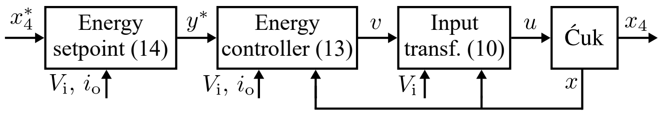


Fig. 2: Block diagram of the proposed closed-loop system.

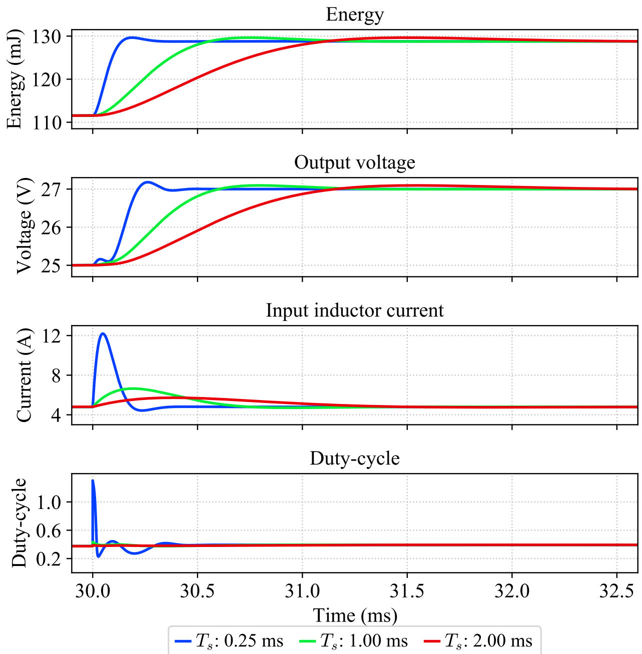


Fig. 3: Simulation results of the closed-loop system for varying settling time and fixed overshoot.

where

$$x_1^* = \frac{P_\mathrm{o}}{V_\mathrm{i}},\ x_2^* = \frac{P_\mathrm{o}}{x_4^*},\ x_3^* = \frac{x_4^*}{N} + V_\mathrm{i}. \tag{15}$$

A block diagram of the proposed control system is shown in Fig. 2. The energy setpoint $y^*$ is obtained based on the output voltage setpoint, according to (14). This setpoint is processed by the energy controller (13) to produce the virtual signal $v$. This virtual signal is then used to obtain the duty-cycle $u$, based on the linearizing law (10).

*3) Controller implementation:* In principle, the state feedback controller (13) can be designed to meet arbitrary overshoot and settling time specifications, which directly shapes the dynamics of the output voltage. In practice, however, the dynamics of the energy controller depends on constraints of the physical converter, mainly current and duty-cycle limitations. This is presented in the simulation results shown in Fig. 3. System (1), the average model of the converter, is simulated with a constant power load. The parameters for the simulation are the same as the experimental converter used to validate the method, and are presented in Section III. The energy controller is used to control the system, and three controllers are designed. All controllers are designed to show the same overshoot, but with settling times of 0.25 ms, 1 ms and 2 ms. As Fig. 3 shows, the energy of the controller is shaped according to the design specifications, and the dynamics of the output voltage is similar to that of the energy. However, the controller with a settling time of 0.25 ms requires a much larger input current, and the duty-cycle would be saturated. Thus, the design of the energy controller is constrained by limitations of the physical converter.

Moreover, in practice, the linearizing feedback law (10) is not exact because model (1) does not account for nonidealities of the real converter. This leads to nonidealities in the double integrator system (12) and results in steady-state errors. This can be overcome by augmenting system (12) with an integrator. Gains $k_1$, $k_2$ and the integrator gain $k_i$ can be found simultaneously via pole placement, and the controller can be designed such that the closed-loop system has two dominant poles. Note that the integrator is added to regulate energy, and not output voltage.

### C. Stability

This section provides a stability analysis of the proposed energy controller. We show that the system is stable around an equilibrium point set by output voltage and output power. Furthermore, we show that the equilibrium point is stable for arbitrary positive output power.

For the Ćuk converter, defining the output as energy results in a system with relative degree of two, and expressions (7) and (8) are one part of the transform $T(x)$. Because the relative degree is less than the order of the system, the system has internal dynamics. The internal dynamics is given by subsystem (6a), and feedback linearization only makes sense if the internal dynamics is stable. Evaluating stability of the internal dynamics requires finding the complete transform $T(x)$ and its inverse. Completing the transform $T(x)$ is achieved by using the condition that $(\partial\phi_i(x)/\partial x)g(x) = 0$. One solution to this condition is

$$\phi_1(x) = L_1 x_1 - \frac{L_2}{N} x_2, \tag{16a}$$

$$\phi_2(x) = C_\mathrm{o} x_4, \tag{16b}$$

yielding the transform $T(x)$:

$$T(x) = \begin{bmatrix} L_1 x_1 - \frac{L_2}{N} x_2 \\ C_\mathrm{o} x_4 \\ \frac{L_1}{2} x_1^2 + \frac{L_2}{2} x_2^2 + \frac{C_\mathrm{c}}{2}\left(\frac{N^2}{N^2+1}\right) x_3^2 + \frac{C_\mathrm{o}}{2} x_4^2 \\ V_\mathrm{i} x_1 - P_\mathrm{o} \end{bmatrix}, \tag{17}$$

which is continuously differentiable. The inverse of $T(x)$, that is $x = T^{-1}(z)$, $z = \begin{bmatrix} z_1 & z_2 & z_3 & z_4 \end{bmatrix}^T$, is found by solving

$$x_1 = \frac{1}{V_\mathrm{i}} z_4 + \frac{P_\mathrm{o}}{V_\mathrm{i}}, \tag{18a}$$

$$x_2 = -\frac{N}{L_2} z_1 + \frac{N L_1}{V_\mathrm{i} L_2} z_4 + \frac{N L_1 P_\mathrm{o}}{V_\mathrm{i} L_2}, \tag{18b}$$

$$\frac{C_\mathrm{c}}{2}\left(\frac{N^2}{N^2+1}\right) x_3^2 = z_3 - \frac{L_1}{2} x_1^2 - \frac{L_2}{2} x_2^2 - \frac{C_\mathrm{o}}{2} x_4^2, \tag{18c}$$

$$x_4 = \frac{1}{C_\mathrm{o}} z_2, \tag{18d}$$

for $x$. Here, we leave (18c) in terms of $x$ due to the length of the resulting expression. Expression (18) shows that the inverse transform exists, because the right-hand side of (18c) is, by definition, always equal to, or larger than zero, such

This article has been accepted for publication in IEEE Journal of Emerging and Selected Topics in Industrial Electronics. This is the author's version which has not been fully edited and content may change prior to final publication. Citation information: DOI 10.1109/JESTIE.2024.3425518



that its square root is always real. Moreover, the inverse is continuously differentiable, and $T(x)$ is bijective if we assume $x_3 \geq 0$. In practice, this is not a restrictive assumption, since $x_3$ is the voltage of the coupling capacitors, and is positive during normal operating conditions.

It is possible to simplify the analysis of the internal dynamics by analyzing the zero dynamics, that is, the internal dynamics when the states of the linear system are assumed controlled and constant. By using feedback linearization, the energy of the converter is controlled and kept at a constant value, and, therefore, the converter's power is zero. In the inverse transform, this means that $z_3$ is constant, and $z_4$ is zero. Noting that $\eta = \begin{bmatrix}\phi_1 & \phi_2\end{bmatrix}^T = \begin{bmatrix}z_1 & z_2\end{bmatrix}^T$, the zero dynamics is given by

$$\dot{z_1} = -\alpha(z_1, z_2) + \frac{z_2}{NC_\mathrm{o}} + V_\mathrm{i}, \tag{19a}$$

$$\dot{z_2} = -\frac{N}{L_2}z_1 - \frac{NL_1P_\mathrm{o}}{L_2V_\mathrm{i}} - \frac{C_\mathrm{o}P_\mathrm{o}}{z_2}, \tag{19b}$$

where $\alpha(z_1, z_2) = x_3$. Because the zero dynamics is a highly nonlinear system, it is difficult to evaluate its stability in an analytical way. However, we show that using the indirect method of Lyapunov also provides useful analytical results. The indirect method of Lyapunov is used to evaluate the stability of the zero dynamics around the equilibrium point given by a certain output voltage and output power, given by (15). Denoting $\bar{x}$ as the equilibrium point, the Jacobian $\tilde{A}$ of system (19) is given by

$$\tilde{A} = \begin{pmatrix} \frac{-(N^2+1)P_\mathrm{o}}{C_\mathrm{c}(\bar{x}_4+NV_\mathrm{i})\bar{x}_4} & \frac{(N^2+1)\bar{x}_4}{N^2C_\mathrm{c}(\bar{x}_4+NV_\mathrm{i})} + \frac{1}{NC_\mathrm{o}} \\ -\frac{N}{L_2} & \frac{P_\mathrm{o}}{C_\mathrm{o}\bar{x}_4^2} \end{pmatrix}. \tag{20}$$

The eigenvalues of $\tilde{A}$ depend on the parameters of the converter, the load, and the output voltage. According to numerical experiments, the eigenvalues of $\tilde{A}$ are a complex-conjugate pair for reasonable design parameters. Cases when the eigenvalues become real are observed when very small or very large values for components are used. One such case is when the coupling capacitor $C_\mathrm{c}$ has a very small value. In practice, this would not result in a realizable converter because, if $C_\mathrm{c}$ is very small, its voltage ripple would be very large, and the converter would not work as expected. Another case where the eigenvalues become real is when the inductors are very large. In practice, making inductors too large is undesirable because they would prevent fast current changes, resulting in a less dynamical system even in the presence of control.

Assuming that the eigenvalues $\lambda_1$ and $\lambda_2$ of $\tilde{A}$ are a complex-conjugate pair, their real part is given by

$$\Re(\lambda_{1,2}) = \left(\frac{NC_\mathrm{c}V_\mathrm{i} + \left(C_\mathrm{c} - (N^2+1)C_\mathrm{o}\right)\bar{x}_4}{2C_\mathrm{c}C_\mathrm{o}\left(NV_\mathrm{i} + \bar{x}_4\right)\bar{x}_4^2}\right)P_\mathrm{o}. \tag{21}$$

In many practical cases, $C_\mathrm{o} \gg C_\mathrm{c}$, and $(N^2+1)C_\mathrm{o}\bar{x}_4 \gg NC_\mathrm{c}V_\mathrm{i}$. This allows simplifying (21) to

$$\Re(\lambda_{1,2}) \approx -\left(\frac{N^2+1}{2C_\mathrm{c}(NV_\mathrm{i} + \bar{x}_4)\bar{x}_4}\right)P_\mathrm{o}. \tag{22}$$

For a positive load power $P_\mathrm{o}$, expression (22) shows that the real part of the eigenvalues lies in the left half of the complex plane, which shows that the zero dynamics (and thus the closed-loop system) is stable around the equilibrium point. Moreover, expression (22) shows that stability is ensured for arbitrary positive values of $P_\mathrm{o}$. The zero dynamics would become unstable if $P_\mathrm{o}$ becomes negative. However, in grid-forming applications, the converter always supplies the grid, and $P_\mathrm{o}$ is always larger than zero.

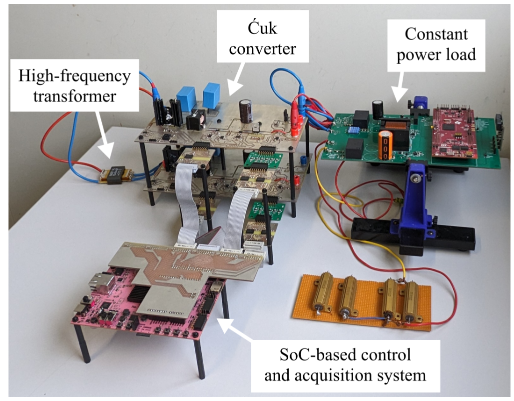


Fig. 4: Experimental setup.

TABLE I: Parts used in the prototype

| Parameter | Value |
|---|---|
| $V_\mathrm{i}$ | 25 V |
| $L_1$ | 100 µH (WE 74437429203101) |
| $L_2$ | 150 µH (WE 74437429203151) |
| $C_1$, $C_2$ | 2 x 4.7 µF (EPCOS B32674D4475K) |
| $C_\mathrm{o}$ | 330 µF (Nichicon UCS2C331MHD) |
| Transformer | Coilcraft NA5871-AL |
| Switching frequency | 100 kHz |
| MOSFETs | Infineon IPP200N25N |
| Inductor current sensor | ACS730KLCTR-40AB-T |
| Output current sensor | ACS712ELCTR-20A-T |
| ADCs | ADC101S021 |
| Digital isolators | SI8641 |

## III. Experimental Results

The proposed controller was verified in an experimental platform, consisting of an isolated Ćuk converter, an embedded controller and a CPL. The experiments focus on two cases: steps in the CPL, and changes in the voltage setpoint of the converter. These are the cases most commonly faced by a grid-forming converter. This section describes the experimental setup and the results obtained.

### A. Experimental setup

Fig. 4 shows the experimental setup used to validate the proposed controller. The setup consists of three main parts: an isolated Ćuk converter, an embedded controller, and a CPL.

The isolated Ćuk converter is built as two separate printed-circuit boards (PCBs) that are coupled through a high-frequency planar transformer. The main parameters of the converter are listed in Table I. A DC bench power supply is used to supply the primary side (input, bottom PCB), and the CPL is connected at the output of the Ćuk converter, on the secondary side (top PCB).

This article has been accepted for publication in IEEE Journal of Emerging and Selected Topics in Industrial Electronics. This is the author's version which has not been fully edited and content may change prior to final publication. Citation information: DOI 10.1109/JESTIE.2024.3425518



The controller is a Zynq-7000 System-on-a-Chip (SoC), comprising a dual-core processor and a field-programmable gate array (FPGA) [30]. The FPGA is used to generate the gate signals for the MOSFETs, and to read the analog-to-digital converters (ADCs). The gate signals are generated based on a triangular carrier. The ADCs are always read when the carrier reaches its maximum value; this allows sampling the average values of the current of the inductor. One core of the dual-core processor is used for real-time control, and the other core is used to provide a command-line-based user interface. The SoC-based controller is used to control the Ćuk converter, and to additionally record voltage and current waveforms. All waveforms shown in this section were acquired with the controller; no filtering is applied to measurements of the ADCs, and the only post-processing applied to the data is conversion from raw ADC measurements to actual measured quantities (voltages and currents). The sampling frequency was set the same as the switching frequency (100 kHz).

The CPL is realized by a separate platform. The platform is a synchronous buck converter, programmed to supply resistive loads at a constant voltage; power steps are achieved by changing the voltage setpoint. The converter uses a switching frequency of 200 kHz, and a state feedback controller with a voltage settling time of 1 ms and minimum overshoot.

### B. Results

The energy-based controller (denoted as EB) is compared with a single-loop state feedback controller (denoted as SFB). The SFB controller was designed based on a linearized model of (1), around an operating point based on nominal output voltage and power. The SFB controller was also augmented with an integrator. The five poles of the linearized system were placed as follows. Two dominant poles were placed based on specifications of settling time and overshoot for a second-order underdamped system. The third, fourth and fifth poles were placed on the real axis with a value of five, ten, and fifteen times the real part of the dominant poles; respectively.

The EB and SFB controllers were designed to achieve a settling time of 2.5 ms and 5% overshoot. For the SFB controller, the converter was linearized based on a voltage setpoint of 25 V and output power of 120 W. All parameters used during design were based on the nominal values of the parts used in the experimental platform (Table I). Moreover, the constant power load has an input capacitance of 150 µF; this capacitance was not added to the output capacitance of the Ćuk converter for design purposes.

In all experiments, the converter was first brought close to the voltage setpoint by slowly increasing the duty-cycle, and then the main controller (EB or SFB) was enabled. For the EB controller, an additional notch filter was added to filter the virtual signal $v$. The reason, and the parameters of the filter, are explained in Section III-B3.

*1) Load steps:* Figs. 5 and 6 show the output voltage of the converter for steps in the power of the CPL. In both cases, the voltage setpoint is 25 V. Fig. 5 shows the output voltage when the power steps from 60 W to 120 W, at 250 ms. With the EB controller, the voltage drops momentarily to 23.8 V, but recovers to within 0.5 V in less than 0.7 ms. The voltage drop of the SFB controller is around 4 V, and the time to recover to within 0.5 V of the setpoint is around 4 ms. Fig. 6 shows the output voltage when the power steps from 120 W to 60 W. The EB controller is able to regulate the voltage to the setpoint within 0.7 ms, while the SFB controller shows larger deviation and slower response.

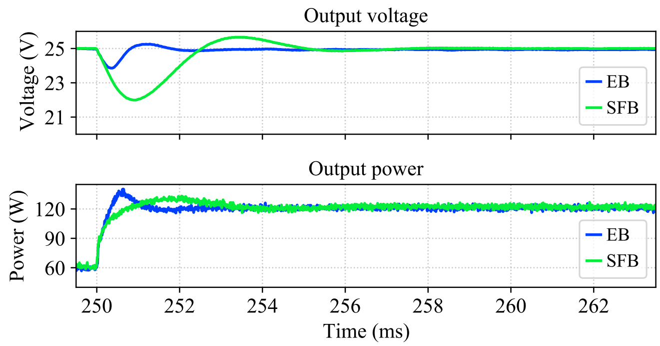


Fig. 5: Output voltage transient when the output power steps from 60 W to 120 W.

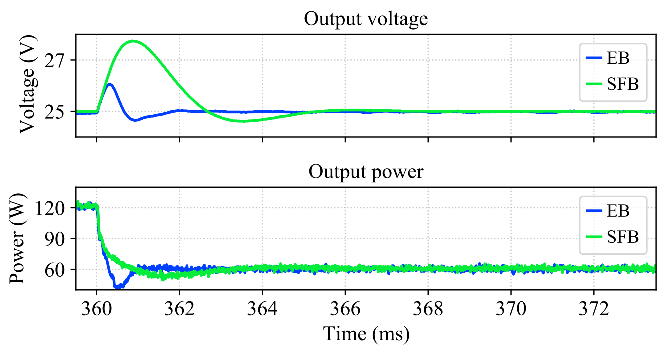


Fig. 6: Output voltage transient when the output power steps from 120 W to 60 W.

*2) Setpoint changes:* Figs. 7 and 8 show experimental results for changes in the setpoint of the output voltage. In both cases, the power of the CPL is set to 120 W. Fig. 7 shows a setpoint change from 25 V to 27 V. When using the EB controller, the voltage is within 2% of the 2 V step in around 3 ms, slightly slower than the designed value of 2.5 ms. Moreover, the overshoot is around 38%, larger than the designed value of 5%. For the SFB controller, the voltage is within 2% in around 6 ms, with an overshoot of around 20%. The same trend is observed when the voltage setpoint changes from 27 V to 25 V, as shown in Fig. 8. Differences between designed and measured settling time and overshoot can be attributed to nonidealities of the real converter and the input capacitance of the CPL. However, the EB controller shows better robustness to model mismatches, given that its settling time is closed to the designed value. Moreover, the transient of the output power appears worse for the EB controller. This behavior is expected and depends on the disturbance rejection capability of the CPL controller. For the same CPL controller, a faster change in its input voltage produces a

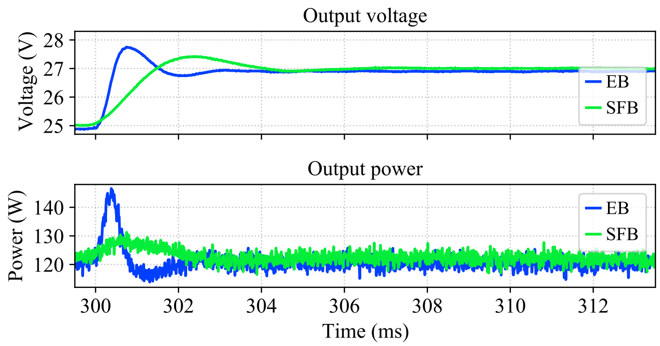


Fig. 7: Output voltage transient when its setpoint changes from 25 V to 27 V, at an output power of 120 W.

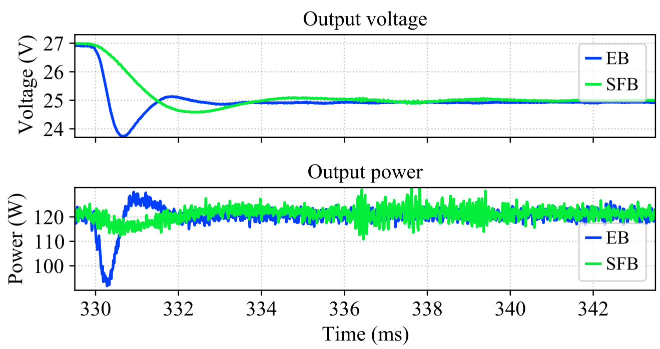


Fig. 8: Output voltage transient when its setpoint changes from 27 V to 25 V, at an output power of 120 W.

stronger disturbance, and the input power profile of the CPL has a larger transient.

*3) Operation at light load:* As discussed in Section II-C, the complex-conjugate eigenvalues of the Jacobian of the zero dynamics indicate oscillations that are not directly observed at the output (which is energy). Moreover, the damping of these oscillations decrease as output power decreases. In the Ćuk converter, these oscillations are not strongly observed at the output voltage but instead in the current of the output inductor, and in the voltage of the coupling capacitors.

One way to avoid these oscillations is to not excite them; that is, generate a control signal that does not resonate with the frequency of these oscillations. A simple way to remove these frequency components from the control signal is to use a notch filter to filter the auxiliary signal $v$. The transfer function $H(s)$ of the notch filter is given by

$$H(s) = \frac{s^2 + \omega_c^2}{s^2 + \frac{\omega_c}{Q}s + \omega_c^2}, \tag{23}$$

where $\omega_c$ is the cut-off frequency and $Q$ is the quality factor. In the EB controller, the cut-off frequency $\omega_c$ is chosen to match the frequency of the oscillations of the internal dynamics, assuming light load conditions. The quality factor $Q$ determines how selective the filter is. If the filter is too selective (high $Q$), the filter is less robust to parametric variations. A low $Q$ renders a filter with a large band, which affects the designed transient response of the EB controller. The cut-off frequency

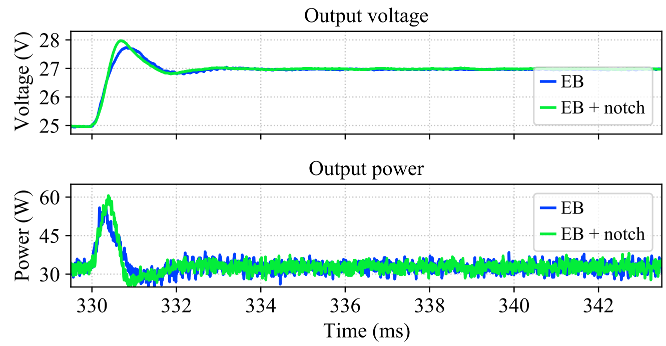


Fig. 9: Output voltage transient when its setpoint changes from 25 V to 27 V, at light load.

and quality factor were obtained experimentally, and set to 3.3 kHz and 0.5 in the EB controller; respectively.

Figs. 9 and 10 show the states of the converter for a change in the voltage setpoint, at light load (approximately 30 W). The EB controller is used to control the converter, and two cases are compared: when no notch filter is used, and when the notch filter is active.

Fig. 9 shows the output voltage and the power of the load. The voltage setpoint is changed from 25 V to 27 V. From the output voltage only, there are only minor differences when the notch filter is enabled. Fig. 10 shows the voltage of the coupling capacitors, and the currents of the input and output inductors. It is possible to see that, without the notch filter, a change in the voltage setpoint causes oscillations that are mostly seen in the voltage of the coupling capacitors. However, these oscillations are damped when the notch filter is used.

## IV. Conclusions

The importance of low-level voltage control for DC/DC converters supplying constant power loads becomes evermore important with the growth of DC microgrids, where grid-forming units are necessary to keep the microgrid stable. This paper presented an energy-based approach for voltage control of an isolated Ćuk converter that is especially interesting for grid-forming applications, since it can naturally handle CPLs. The proposed approach leads to a single-loop controller that can be designed based on linear control methods.

The main drawback of the method is the number of measurements required, especially the more expensive current measurements. Further research will explore the use of observers to replace these measurements. Moreover, the energy state feedback controller can be replaced with more advanced controllers. One option is to use model-predictive control, which could ensure that feedback linearization is always valid, by accounting for constraints on the duty-cycle.

## References

[1] S.-E. Razavi, E. Rahimi, M. S. Javadi, A. E. Nezhad, M. Lotfi, M. Shafie-khah, and J. P. Catalão, "Impact of distributed generation on protection and voltage regulation of distribution systems: A review," *Renew. Sustain. Energy Rev.*, vol. 105, pp. 157–167, 2019.

This article has been accepted for publication in IEEE Journal of Emerging and Selected Topics in Industrial Electronics. This is the author's version which has not been fully edited and content may change prior to final publication. Citation information: DOI 10.1109/JESTIE.2024.3425518



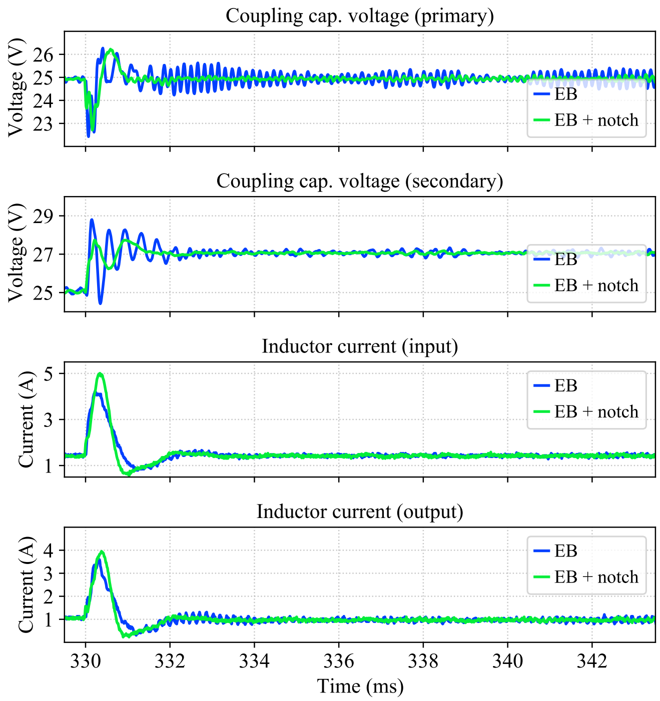


Fig. 10: Voltage of coupling capacitors and current of input and output inductors, when the setpoint for the output voltage changes from 25 V to 27 V, at light-load.

[2] K. E. Antoniadou-Plytaria, I. N. Kouveliotis-Lysikatos, P. S. Georgilakis, and N. D. Hatziargyriou, "Distributed and decentralized voltage control of smart distribution networks: Models, methods, and future research," *IEEE Trans. Smart Grid*, vol. 8, no. 6, pp. 2999–3008, 2017.
[3] A. Muhtadi, D. Pandit, N. Nguyen, and J. Mitra, "Distributed energy resources based microgrid: Review of architecture, control, and reliability," *IEEE Trans. Ind. Appl.*, vol. 57, no. 3, pp. 2223–2235, 2021.
[4] A. Hirsch, Y. Parag, and J. Guerrero, "Microgrids: A review of technologies, key drivers, and outstanding issues," *Renew. Sustain. Energy Rev.*, vol. 90, pp. 402–411, 2018.
[5] S. Ullah, A. M. Haidar, P. Hoole, H. Zen, and T. Ahfock, "The current state of distributed renewable generation, challenges of interconnection and opportunities for energy conversion based DC microgrids," *J. Clean. Prod.*, vol. 273, p. 122777, 2020.
[6] S. Beheshtaein, R. M. Cuzner, M. Forouzesh, M. Savaghebi, and J. M. Guerrero, "DC microgrid protection: A comprehensive review," *IEEE J. Emerg. Sel. Top. Power Electron.*, 2019.
[7] Y. Neyret, "DC microgrids: Principles and benefits," 2021. [Online]. Available: https://www.dc.systems/assets/public/DC-Systems-White-Paper.pdf
[8] E. L. Carvalho, A. Blinov, A. Chub, P. Emiliani, G. de Carne, and D. Vinnikov, "Grid integration of DC buildings: Standards, requirements and power converter topologies," *IEEE Open J. Power Electron.*, vol. 3, pp. 798–823, 2022.
[9] X.-K. Liu, Y.-W. Wang, Z.-W. Liu, and Y. Huang, "On the stability of distributed secondary control for DC microgrids with grid-forming and grid-feeding converters," *Automatica*, vol. 155, p. 111164, 2023.
[10] S. Sharma, V. M. Iyer, S. Bhattacharya, K. Zou, and J. Kikuchi, "Droop-based distributed secondary control method with reduced communication complexity for radial DC microgrids," *IEEE J. Emerg. Sel. Top. Ind. Electron.*, vol. 4, no. 3, pp. 969–981, 2023.
[11] W. Xie, M. Han, W. Cao, J. M. Guerrero, and J. C. Vasquez, "System-level large-signal stability analysis of droop-controlled DC microgrids," *IEEE Trans. Power Electron.*, vol. 36, no. 4, pp. 4224–4236, 2021.
[12] A. Ramanath, A. Kshirsagar, S. Thamballa, and N. Mohan, "Equivalent modeling, design and analysis of integrated magnetics Ćuk converter," in *2019 NAPS*, 2019.
[13] A. Ramanath, A. Kshirsagar, and N. Mohan, "Analysis of current ripple in Ćuk converter topologies - a novel approach," in *2018 IEEE PEDES*, 2018, pp. 1–6.
[14] J. L. Seguel, S. I. Seleme, and L. M. F. Morais, "Comparative study of Buck-Boost, SEPIC, Cuk and Zeta dc-dc converters using different MPPT methods for photovoltaic applications," *Energies*, vol. 15, no. 21, 2022.
[15] G. Gámez E., C. A. Palafox S., H. Mendivil C., J. A. Beristáin J., and J. Pérez R., "Contribution to the analysis and design of the Cuk converter for the transfer of photovoltaic solar energy to batteries," in *2019 IEEE ROPEC*, 2019, pp. 1–6.
[16] P. K. Maroti, S. Padmanaban, P. Wheeler, F. Blaabjerg, and M. Rivera, "Modified high voltage conversion inverting Cuk DC-DC converter for renewable energy application," in *2017 IEEE SPEC*, 2017.
[17] B. Pawar, E. I. Batzelis, S. Chakrabarti, and B. C. Pal, "Grid-forming control for solar PV systems with power reserves," *IEEE Trans. Sustain. Energy*, vol. 12, no. 4, pp. 1947–1959, 2021.
[18] M. E. Elkhatib, W. Du, and R. H. Lasseter, "Evaluation of inverter-based grid frequency support using frequency-watt and grid-forming PV inverters," in *2018 IEEE PESGM*, 2018, pp. 1–5.
[19] Z. Chen, "PI and sliding mode control of a Cuk converter," *IEEE Trans. Power Electron.*, vol. 27, no. 8, pp. 3695–3703, 2012.
[20] Y. Wu, A. Isidori, R. Lu, and H. K. Khalil, "Performance recovery of dynamic feedback-linearization methods for multivariable nonlinear systems," *IEEE Trans. Autom. Control*, vol. 65, no. 4, pp. 1365–1380, 2020.
[21] A. Isidori, *Nonlinear Control Systems*. London: Springer, 1995.
[22] W. He, M. M. Namazi, T. Li, and R. Ortega, "A state observer for sensorless control of power converters with unknown load conductance," *IEEE Trans. Power Electron.*, vol. 37, no. 8, pp. 9187–9199, 2022.
[23] J. L. Flores, J. L. B. Avalos, and C. A. B. Espinosa, "Passivity-based controller and online algebraic estimation of the load parameter of the DC-to-DC power converter Cuk type," *IEEE Lat. Am. Trans.*, vol. 9, no. 1, pp. 784–791, 2011.
[24] H. Rodriguez, R. Ortega, and G. Escobar, "A new family of energy-based non-linear controllers for switched power converters," in *IEEE 2001 ISIE*, vol. 2, 2001, pp. 723–727 vol.2.
[25] R. Ortega and P. Borja, *Passivity-Based Control*. Springer International Publishing, 2021, pp. 1684–1691.
[26] H. Ramírez, D. Sbarbaro, and R. Ortega, "On the control of non-linear processes: An IDA–PBC approach," *J. Process Control*, vol. 19, no. 3, pp. 405–414, 2009.
[27] R. Ortega, A. van der Schaft, B. Maschke, and G. Escobar, "Interconnection and damping assignment passivity-based control of port-controlled Hamiltonian systems," *Automatica*, vol. 38, no. 4, pp. 585–596, 2002.
[28] C. A. Ramos-Paja, D. G. Montoya, and J. D. Bastidas-Rodríguez, "Sliding-mode control of a CuK converter for voltage regulation of a dc-bus," *Sustain. Energy Technol. Assess.*, vol. 42, p. 100807, 2020.
[29] J. Knight, S. Shirsavar, and W. Holderbaum, "An improved reliability cuk based solar inverter with sliding mode control," *IEEE Trans. Power Electron.*, vol. 21, no. 4, pp. 1107–1115, 2006.
[30] M. Guerreiro, S. Kharade, P. Dos Santos, and S. Liu, "Power electronics control with system-on-a-chip-based platforms," in *2022 IEEE 20th PEMC*, 2022, pp. 353–359.